Phase diagram for excess electrons in simple fluids

Kevin Leung and David Chandler
Department of Chemistry, University of California, Berkeley, California 94720
(Received 12 October 1993)

We analyze a model for a thermally equilibrated electron in a static disordered environment. The model provides a caricature of excess electrons in simple liquids. We show that the self-consistent Gaussian approximation to the model can be treated analytically in the different limits of weak and strong coupling to the disorder. In cases of strong coupling, the treatment predicts electron localization consistent with Lifshitz trap scaling. This behavior can be the result of either excluded volume interactions or attractive interactions between the electron and the random sites (i.e., atoms) in the system. In the former case, the Lifshitz traps are voids; in the latter, they are local regions with atomic density in excess of the mean. In the case of weak coupling, the electronic behavior is dominated by extended states, and our treatment is consistent with standard perturbation theory. The theory thus correctly interpolates between different regimes. As a result, it provides a means to examine the competition between different electron-solvent interactions, and the resulting changes from one regime to another. We derive a phase diagram for the regions of crossover between weak coupling and strong coupling. The phase diagram is of a re-entrant form where the weak-coupling regime can result from a competition between repulsive and attractive interactions. Within this regime, over a narrow range of atomic densities, it is shown that the electron mobility can be extremely high.

PACS number(s): 61.20.−p, 71.10.+x, 71.25.Mg, 71.55.Jv

I. INTRODUCTION

The remarkably varied behavior of excess electrons in simple liquids has attracted attention, both experimentally [1,2] and theoretically [2,3]. In this paper, we analyze a model that can explain many of the qualitative observations. The self-consistent Gaussian approximation to the model coincides with a theory presented several years ago [4]. Several numerical applications of this theory have been made to interpret the structure and mobility of excess electrons in nonpolar and polar liquids [5–13]. The current paper provides an analytical treatment. We predict a phase diagram for the crossover between regions of high electron mobility (dominated by extended states) and regions of low mobility (dominated by localized states). Much of what we have to say pertains to the general problem of a quantal particle coupled to static disorder.

We assume that an electron couples to a liquid of simple closed shell atoms or molecules through a local pseudopotential field. This field is irregular due to the disordered arrangements of atoms in such a system. Closed shell atoms will repel excess electrons, due to the exclusion principle. They may also attract excess electrons, due to polarization. As such, the potential landscape for the electron can have regions of high energy, nearly impenetrable to the excess electron, and it can have other regions of low energy that attract the electron.

Irregularity throughout the landscape will cause low energy states of an excess electron to be localized. This is the case of strong coupling that will necessarily dominate the behavior of excess electrons at sufficiently low temperatures. The opposite regime of low coupling dominates the behavior at high temperatures. We develop in this paper an analytical treatment of both the strong-coupling and weak-coupling regimes. We also describe how in certain cases, the effects of the repulsive and attractive interactions compete and cancel each other. This cancellation phenomenon has often been cited as the cause of high electron mobilities in some of the rare gas fluids [2,10,14]. It is also known in other contexts. For example, the phenomenon gives rise to the Ramsauer-Townsend effect in two body scattering [15]. It also provides the mechanism for extended states and conductivity in the random dimer model [16].

Experiments on excess electrons in liquids are performed at finite temperatures. Therefore, our theoretical analysis is carried out in the canonical ensemble. In the microcanonical ensemble, there is a clear demarcation between extended and localized behavior as a function of the energy of a single electron. The microcanonical diffusion constant, for example, is zero for those ranges of energy where states are localized, and it is nonzero for those energies where states are extended. (Equivalently, there are well defined localization transitions for a zero temperature many body system of noninteracting electrons as a function of chemical potential.) For a thermally equilibrated excess electron, however, observables exhibit smeared manifestations of such transitions.

Even at finite temperatures, a liquid environment is static in as much as the liquid atoms move much slower than do the electrons. Electron localization occurs only to the extent that the solvent is not dynamic. In the treatment we follow, the liquid exhibits no dynamics. In other words, the extreme adiabatic approximation is employed. This static model of liquid disorder is a reason-

able approximation for nearly all nonpolar liquids. The diffusion constants for the slowest electrons in such systems are typically 10^2 times those of the solvent atoms. The exception is liquid helium at temperatures below 5 K, where the electron diffusion constant approaches that of the helium atoms. In that case, a significant mechanism for diffusion of the electron is provided by the motions of the surrounding atoms. Above those low temperatures, and for other nonpolar liquids, the so-called "bubble states" are effectively stationary. Diffusion of the electron is due primarily to diffraction made possible through access to extended states.

The model and the self-consistent Gaussian approximation we use to analyze the electronic behavior caused by static disorder is presented in Sec. II. The analysis of the theory is generally complicated, requiring some degree of numerical computation. In the limits of weak and strong coupling, however, the analysis can be done analytically. We demonstrate the analytical treatment in Sec. III where we consider only the effects of random exclusion. The crossover between the two regimes is located approximately, by extrapolating from those limits. In Sec. IV, we consider the cases where both attracting and excluding interactions are present. Here, a phase diagram is predicted in which the boundary between weak and strong coupling is of a re-entrant form. The weak coupling arises from a cancellation between attractions and repulsions. A brief summary and a discussion of the limitations inherent to our model are given in Sec. V. Appendices provide several of the mathematical steps omitted from the main text.

II. THEORY

A. The model

We imagine an electron coupled to a liquid through a very simple pseudopotential. This potential expels the electron from distances closer than some length, l, to the center of any atom in the liquid. Outside these excluded regions, the electron may be attracted to atoms with a pair potential $u(r)$. The pseudopotential is intended as a caricature, valid for reasonably low energies and reasonably long length scales. For such circumstances, the atomic density, $\rho(\mathbf{r})$, provides a convenient description of liquid configurations. This quantity is a random field. We assume that the resulting disorder is quenched (i.e., adiabatic) on the time scale of the electron's diffusive motion. Further, we assume that electrons are uncorrelated to each other and are equilibrated to the disorder.

As a result of these assumptions, the appropriate generating functional is the single electron partition function

$$Z \equiv e^{-\beta\Delta\mu} = \int \mathcal{D}\mathbf{r}[\tau] \int \mathcal{D}\rho(\mathbf{R})\, P[\rho(\mathbf{R})] \prod_{|\mathbf{R}'-\mathbf{r}(\tau)|<l} \delta[\rho(\mathbf{R}')] \exp\left\{ S_0[\mathbf{r}(\tau)] - \frac{1}{\hbar}\int_0^{\beta\hbar} d\tau \int d\mathbf{R}\, \rho(\mathbf{R}) u[\mathbf{r}(\tau)-\mathbf{R}] \right\}. \tag{2.1}$$

In the above equation, $P[\rho(\mathbf{R})]$ denotes the probability distribution functional for the density fields of the pure liquid solvent, $\mathbf{r}(\tau)$ is the position of the electron along the imaginary-time path at imaginary time τ, and the product of δ functions ensures that there is no solvent density within the distance of closest approach of the cyclic electron path $\mathbf{r}(\tau)$, $0 < \tau < \beta\hbar$;

$$S_0[\mathbf{r}(\tau)] = -\frac{1}{\hbar}\int_0^{\beta\hbar} d\tau\, \frac{1}{2} m_e \dot{\mathbf{r}}^2 \tag{2.2}$$

is the Euclidean-time action of a free electron, and m_e is the electronic mass. The quantity $\Delta\mu = \beta^{-1}\ln Z$ is the chemical potential or excess free energy of an electron in the fluid. The path integration differential, $\mathcal{D}r(\tau)$, includes a constant such that $\Delta\mu \to 0$ as $\rho \to 0$. In other words, the chemical potential reference state is the electron uncoupled from the solvent.

Equation (2.1) is an expression for an equilibrium or *annealed* partition function. Electrons *equilibrated* to quenched or static disorder obey the principle of self-averaging. As such, it can be shown that for uncorrelated electrons in the thermodynamic limit, quenched averaging is equivalent to annealed averaging [17]. The partition function associated with annealed averaging, Eq. (2.1), is easier to evaluate than that for quenched averaging. Thus, Eq. (2.1) is the appropriate partition function based upon both principle and convenience.

This strategy is satisfactory for the treatment of both structural and dynamical properties of independent electrons equilibrated to classical liquid disorder. The processes leading to equilibration, however, involve interplay between electronic and liquid dynamics [18]. This nonequilibrium relaxation is beyond the scope of the static liquid model we adopt.

Our focus is on the region where the thermal wavelength of the electron

$$\lambda = \sqrt{\beta\hbar^2/m_e}$$

far exceeds all other relevant length scales, including the correlation length of the liquid disorder. At long enough length scales, the statistics of the solvent density is Gaussian. Owing to the large value of λ, we assume a Gaussian description is reasonable at all pertinent scales. Hence, the disorder is characterized by the averaged density, ρ, and the second moment,

$$\langle \delta\rho(\mathbf{r})\delta\rho(\mathbf{r}')\rangle = \chi(|\mathbf{r}-\mathbf{r}'|). \tag{2.3}$$

Given this assumption, the partition function [Eq. (2.1)] and the implied correlation functions can be estimated from results of the Li-Kardar method [19]. That procedure can be carried through in the $l \to 0^+$ limit [20]. Extrapolating to finite l gives

$$\rho[g(r) - 1] = \omega * c * \chi(r), \tag{2.4}$$

where

$$g(r) = 0, \; r < l, \tag{2.5}$$

and

$$c(r) = -\beta u(r), \; r > l. \tag{2.6}$$

Here, $\rho g(r)$ is the average density at $\mathbf{r}$ given an electron is at the origin, $*$ denotes convolution in real space, and $\omega(r)$ is the time-averaged correlation function between two points on the electron path:

$$\omega(|\mathbf{r}|) = \frac{1}{\beta\hbar}\int_0^{\beta\hbar} d\tau \, \langle \delta(\mathbf{r} - \mathbf{r}(\tau) + \mathbf{r}(\tau')) \rangle. \tag{2.7}$$

Equations (2.4)–(2.6) are derived neglecting deviations of the electron pair structure from its average, $\langle \delta(\mathbf{r} - \mathbf{r}(\tau) + \mathbf{r}(\tau')) \rangle$. See Ref. [20]. One requires a self-consistent theory to determine this correlation function.

B. Self-consistent Gaussian treatment

Equations (2.4)–(2.6) are consistent with

$$\begin{aligned} Z \approx & \int \mathcal{D}\rho(\mathbf{R}) \, P[\rho(\mathbf{R})] \int \mathcal{D}\mathbf{r}[\tau] \, \exp\{S_o[\mathbf{r}(\tau)] \\ & + \frac{1}{\hbar}\int_0^{\beta\hbar} d\tau \int d\mathbf{R} \, \rho(\mathbf{R}) c(\mathbf{r}(\tau) - \mathbf{R})\} \\ = & \int \mathcal{D}\mathbf{r}(\tau) \exp\{S_o[\mathbf{r}(\tau)] + S_I[\mathbf{r}(\tau)]\}, \end{aligned} \tag{2.8}$$

where

$$S_I[\mathbf{r}(\tau)] = \rho\hat{c}(0) - \frac{1}{2}\int_0^{\beta\hbar} \frac{d\tau}{\beta\hbar} \int_0^{\beta\hbar} \frac{d\tau'}{\beta\hbar} v(|\mathbf{r}(\tau) - \mathbf{r}(\tau')|), \tag{2.9}$$

and

$$v(r) = -c * \chi * c(r) \tag{2.10}$$

is the influence functional potential. Equations (2.8)–(2.10) provide a partition function from which $\langle \delta(\mathbf{r} - \mathbf{r}(\tau) + \mathbf{r}(\tau')) \rangle$ can be computed. To arrive at self-consistency, we enforce the condition that the resulting $\omega(r)$ gives [via Eq. (2.4)] an expression for $c(r)$ which is consistent with it.

The influence functional in Eq. (2.9) resembles that which Feynman obtained by integrating out the dynamical phonon bath present in the Fröhlich Hamiltonian [21]. Unlike Feynman's case, however, the influence functional couplings, $v(r)$, are independent of time and hence long ranged in time. Also unlike Feynman's case, $v(r)$ is not only a functional of the electronic environment. It depends as well upon the electronic structure. These features arise, respectively, from the static nature of the disorder and the nonlinear nature of the model we consider. They lead, as we show below, to manifestations of localization. It is well known and our results are consistent with the fact that localization is different in important ways from polaronic self-trapping. The latter is caused by coupling to a dynamical phonon bath. Despite the differences, the analysis we provide establishes a useful analogy between localization in a static medium and the behavior of polarons.

To compute the thermal averaging, we follow Feynman's variational approach [21] and minimize the excess chemical potential through first order in $\Delta S[\mathbf{r}(\tau)]$, i.e.,

$$\beta\Delta\mu = \beta\Delta\mu_{\text{ref}} - \langle \Delta S[\mathbf{r}(\tau)] \rangle_{\text{ref}}, \tag{2.11}$$

with respect to the most general Gaussian influence function

$$S_{\text{ref}}[\mathbf{r}(\tau)] = -\sum_{n=1}^{\infty} \gamma_n |\mathbf{r}_n|^2, \tag{2.12}$$

where

$$\begin{aligned} \Delta S[\mathbf{r}(\tau)] &= S_I[\mathbf{r}(\tau)] - S_{\text{ref}}[\mathbf{r}(\tau)], \\ \mathbf{r}_n &= \frac{1}{\beta\hbar}\int_0^{\beta\hbar} d\tau \, \mathbf{r}(\tau) \cos(\Omega_n \tau), \end{aligned}$$

Ω_n is the Matsubara frequency $2\pi n(\beta\hbar)^{-1}$, and $\{\gamma_n\}$ is an infinite set of variational parameters. With this reference action, our variational treatment is also equivalent to setting to zero the first order correction to the mean square:

$$\begin{aligned} \langle |\mathbf{r}_n|^2 \rangle^{(1)} &\equiv \langle |\mathbf{r}_n|^2 \Delta S[\mathbf{r}(\tau)] \rangle_{\text{ref}} - \langle |\mathbf{r}_n|^2 \rangle_{\text{ref}} \langle \Delta S[\mathbf{r}(\tau)] \rangle_{\text{ref}} \\ &= 0. \end{aligned}$$

The results of the optimization are [4]

$$\langle |\mathbf{r}_n|^2 \rangle = \frac{3}{\beta m_e \Omega_n^2 + \gamma_n} \tag{2.13}$$

and

$$\begin{aligned} \gamma_n = -\frac{1}{6\pi^2}\int_0^{\beta\hbar} d\tau \, (1 - \cos\Omega_n\tau) \\ \times \int_0^{\infty} dk \, k^4 \hat{v}(k) \exp[-k^2\xi(\tau)]. \end{aligned} \tag{2.14}$$

Finally, $\omega(r)$ in Eq. (2.7) is computed using this reference action to give

$$\hat{\omega}(k) = \frac{1}{\beta\hbar}\int_0^{\beta\hbar} d\tau \, \exp[-k^2\xi(\tau)], \tag{2.15}$$

where

$$\xi(\tau) \equiv R^2(\tau)/6, \tag{2.16}$$

and

$$R^2(\tau) = \langle |\mathbf{r}(\tau) - \mathbf{r}(0)|^2 \rangle = 12 \sum_{n=1}^{\infty} \frac{1 - \cos(\Omega_n \tau)}{\beta m_e \Omega_n^2 + \gamma_n}. \quad (2.17)$$

Equations (2.4)–(2.6), (2.13)–(2.17) are solved self-consistently [22]. Approximate analytical methods used to solve this set of coupled integral equations are given in Sec. III and are discussed in more detail in Appendix A.

C. Real time dynamics

The solutions to these equations, as we will show, yield a variety of behaviors. When dominated by localized low energy states, the electron is hardly mobile. On the other hand, it is possible for the electron to couple weakly to the liquid, even when the bare pseudopotentials seem appreciable. In that case the electron diffuses rapidly. To analyze these real time behaviors, one may analytically continue the imaginary time Eqs. (2.13)– (2.17) [8]:

$$\xi_>(t) = \frac{1}{6}\langle \mathrm{T}|\mathbf{r}(t) - \mathbf{r}(0)|^2 \rangle = -\frac{1}{\pi}\int_0^\infty d\omega\, \mathrm{Im}\big(\beta\hbar/[\beta m_e \omega^2 + \hat{\gamma}(\omega)]\big) \times [\coth(\beta\hbar\omega/2)\,(1 - \cos\omega t) + i \sin\omega t], \quad (2.18)$$

$$\hat{\gamma}(\omega) = -\frac{2}{\beta\hbar}\int_0^\infty dt\,(1 - e^{i\omega t})\mathrm{Im} g_>(t) = -\frac{1}{i\beta\hbar}\left\{ \int_{C_1} dt\,(1 - e^{i\omega t}) g_>(t) + \int_{C_2} dt\,[1 - e^{-\beta\hbar\omega + i\omega t}] g_>(t) \right\}, \quad (2.19)$$

and

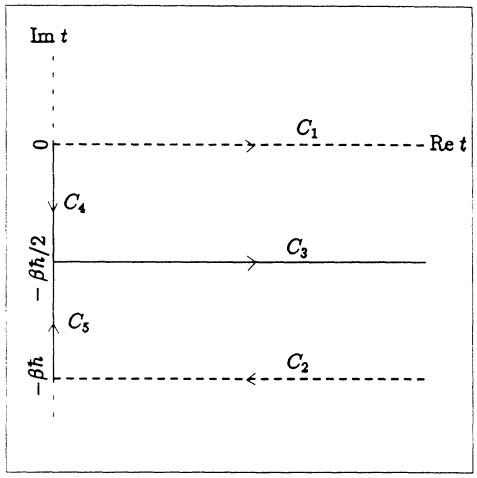

FIG. 1. Contours in the complex time plane used in Eqs. (2.19) and (2.22). The dashed lines (C_1 and C_2) are the contours used in Eq. (2.19) and the solid lines (C_3, C_4, and C_5) run through the lines along which $g_>(t)$ is real.

$$g_>(t) = \frac{1}{6\pi^2}\int_0^\infty dk\, k^4 \hat{v}(k) \exp[-k^2 \xi_>(t)], \quad (2.20)$$

where T is the time-ordering operator and the contours C_1 and C_2 are shown in Fig. 1. The diffusion constant is given by

$$\frac{1}{D} = \lim_{\omega \to 0} \frac{\hat{\gamma}(\omega)}{i\omega}. \quad (2.21)$$

Equation (2.19) involves integrating over a complex contour. Since $\xi_>(t)$ is analytic on the strip bounded by $0 < \mathrm{Im}\, t < \beta\hbar$, we may distort the contour onto C_3. $\xi_>(t)$ is real along C_3, and this procedure minimizes oscillations in the integrals. Equation (2.19) becomes

$$\hat{\gamma}(\omega) = -\frac{1}{i\beta\hbar}\left[\int_{C_3 \cup C_4} dt\,(1 - e^{i\omega t}) g_>(t) - \int_{C_3 \cup C_5} dt\,(1 - e^{-\beta\hbar\omega + i\omega t}) g_>(t) \right] = -\frac{2}{\beta\hbar}\left[i \sinh\left(\frac{\beta\hbar\omega}{2}\right) \int_0^\infty dt\, e^{i\omega t} g_>\left(t - \frac{i\beta\hbar}{2}\right) + \int_0^{\beta\hbar/2} d\tau\,(\cosh\omega\tau - 1) g_>(-i\tau) \right]. \quad (2.22)$$

These equations couple low and high frequency motions. The full solution is prohibitive, though we will discuss how approximate methods can be used to analyze it.

This theory of uncorrelated electrons in liquid matter (or disordered matter in general) is based upon older theories of solvation, principally the reference interaction site model (RISM) [23]. Due to this connection, and due to the analogy with Feynman's treatment of the polaron problem, the theory has been called the RISM-polaron theory [4–13].

III. EFFECTS OF EXCLUDED VOLUME INTERACTION

In this section we consider the model for the case where the attractive potential tail, $u(r)$, is zero. Only exclusion forces remain between the electron and fluid particles.

The quantity $R(\beta\hbar/2)$ obtained from Eq. (2.17) is a measure of the physical size of the thermal electron. In Figs. 2 and 3, we examine this quantity as computed

numerically from Eqs. (2.4)–(2.6) and (2.13)–(2.17). We model the solvent as hard spheres with the Percus-Yevick structure factor [24] for $\chi(r)$, and we take $l = 0.5\sigma$. The plots indicate the occurrence of two distinct types of behavior. At small λ, $R(\beta\hbar/2)$ takes on the scaling form of a free electron,

$$R_{\text{free}}(\beta\hbar/2) = \sqrt{\frac{3}{4}}\lambda.$$

As λ increases, $R(\beta\hbar/2)$ experiences a crossover and then assumes a different functional dependence with λ. We call the regions of phase space associated with the two distinct types of behavior the *weak-coupling* and *strong-coupling* regimes, respectively. In the case of helium, for example, the crossover occurs at physically realizable temperatures. In particular, with $\sigma = 2.6$ Å (a reasonable atomic diameter for helium), $\lambda = 25\sigma$ implies $T \approx 22$ K, whereas at $\lambda = 50\sigma$, T is down to approximately 5.4 K. The liquid-gas critical temperature for helium is about 5 K. At the temperatures and densities considered in Fig. 2 and 3, the classical Percus-Yevick model of that fluid is an accurate enough caricature.

One sees from Fig. 2 that, in the crossover region, the electron size is a nonmonotonic function of temperature. This behavior could be studied experimentally for electrons in gaseous supercritical helium, perhaps through infrared absorption spectroscopy [25]. The nonmonotonic behavior has been observed numerically in the context of an isomorphic problem—the behavior of freely-jointed polymers equilibrated to a system of random quenched obstacles. The polymer mass N in that case coincides with λ^2 or β in the current case. A qualitative understanding of the crossover region can be derived by extrapolating from the two asymptotic regimes. Figure 3 plots $R(\beta\hbar/2)$ vs ρ and shows that (a) $R(\beta\hbar/2)$ is an increasing function of λ in both asymptotic regions; and (b) the crossover point shifts to lower densities as λ increases. From these facts we deduce there must be crossings between different isotherms as ρ varies, and such crossings lead to the nonmonotonic behavior shown in Fig. 2. The location of the crossover region can be estimated by extrapolating from asymptotic results, as will be estimated shortly.

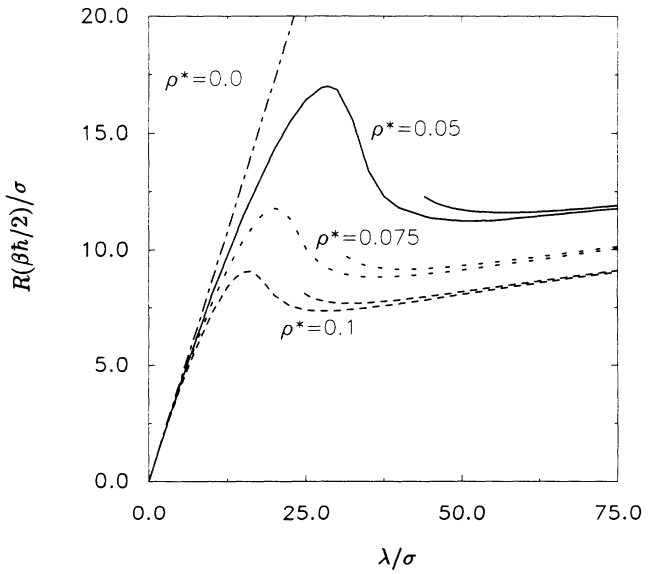

FIG. 2. $R(\beta\hbar/2)$ as a function of λ: $\rho^* = \rho\sigma^3 = 0.05$ (solid line), 0.075 (dashed line), and 0.1 (long-dashed line). In each case, $l = 0.5\sigma$. The abbreviated lines are the asymptotic results from Eq. (3.12).

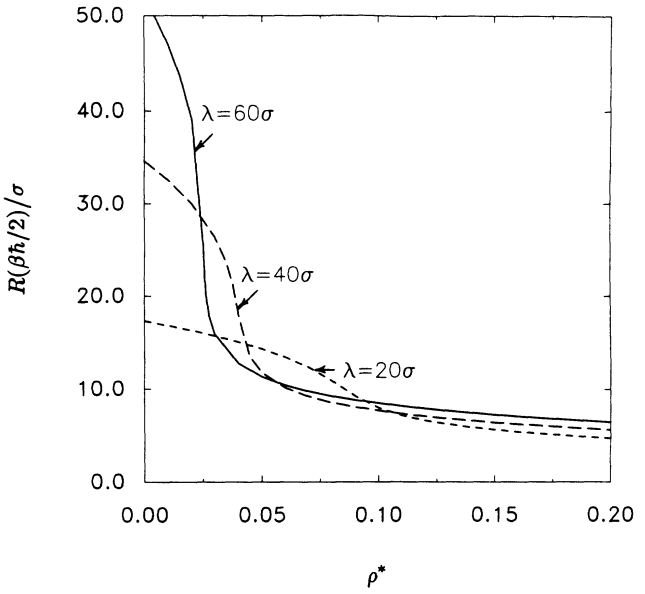

FIG. 3. $R(\beta\hbar/2)$ as a function of ρ at $l = 0.5\sigma$. $\lambda/\sigma = 60$ (solid line), 40 (long-dashed line), and 20 (dashed line).

A. Weak-coupling regime

For purely excluded volume interactions, the extent of electron-solvent scattering increases with density. At low enough solvent density, high enough temperature, or small enough l, one expects the thermal electron to resemble a free quantal particle. In that weak-coupling case, $\xi(\tau)$ assumes the form

$$\xi(\tau) \approx \frac{\lambda^2\tau}{2\beta\hbar}\left(1 - \frac{\tau}{\beta\hbar}\right). \tag{3.1}$$

Nichols and Chandler [8] have derived expressions for $c(r)$ for such a quasifree thermal electron in the ideal gas limit. We extend this calculation to the case for non-trivial solvent structure. In Appendix B, we argue that, for large enough λ, it is sufficient to write

$$c(r) = c_\delta\delta(r-d)/4\pi r^2\,,\ r < l, \tag{3.2}$$

just as in Ref. [8]. With this form for $c(r)$, we show in Appendix A that

$$\beta\Delta\mu \sim \frac{\pi\rho\lambda^2 l}{2K}, \tag{3.3}$$

where

$$K = \frac{2}{\pi l}\int_0^\infty dk\,\hat{S}(k)\left(\frac{\sin kl}{k}\right)^2, \tag{3.4}$$

with $\hat{S}(k) = \hat{\chi}(k)/\rho$ denoting the fluid structure factor. For the hard sphere model of the solvent, $K < 1$, decreases with solvent density ρ, and approaches unity in the ideal gas limit.

In the ideal gas limit, Eq. (3.3) has the functional form of the Springett-Jortner-Cohen expression [26] based on the Wigner-Seitz theory [27], for excess electrons in infinitely dilute hard sphere fluids,

$$\beta\Delta\mu_{\rm WS} = 2\pi\beta\hbar^2\rho l_{\rm WS}m_e^{-1}, \tag{3.5}$$

provided that the scattering length of the electron-solvent pseudopotential $l_{\rm WS}$ is proportional to the distance of closest approach l. In this weak-coupling regime, the chemical potential of the excess electron is system-specific and increases monotonically with l. Its proportionality to $\rho\lambda^2 l$ is easily understood as $\lambda^2 \propto \beta$ is proportional to the number of units on the isomorphic polymer, and l is the only other relevant length scale in the small ρ limit.

B. Strong-coupling regime—Lifshitz traps

With strong coupling to disorder, a different behavior is found. In particular, we show that in this case, excess electrons favor cavities containing low solvent density. In such cavities, known as Lifshitz traps [28], one expects

$$\beta\Delta\mu \sim \beta c\hbar^2/m_eR^2 + b\rho R^d,$$

where c and b are of order unity, and $R \approx R(\beta\hbar/2)$ is the typical distance across a cavity. The first term in this estimate of $\beta\Delta\mu$ is a kinetic energy contribution. The second term arises from the free energy cost to create a void of volume R^d in the fluid. It is athermal. Balancing both terms gives

$$R \sim (\beta/\rho)^{1/(d+2)}. \tag{3.6}$$

This well-known phenomenological argument predicts that the optimal cavity size R scales as $T^{-1/5}$ at low temperatures in three dimensions. Such scaling behavior has been derived with microscopic methods by Luttinger *et al.* [29–31] in the case of random uncorrelated short-ranged repulsive scatterers. In the strong-coupling limit, the RISM-polaron theory [Eq. (2.4)–(2.6), (2.13)–(2.17)] reduces to an analytically tractable form yielding Lifshitz's results as well.

We begin by assuming the dominance of ground states, as is appropriate for large enough λ. In that case, $\xi(\tau)$ is independent of τ, except for τ very close to 0 (or $\beta\hbar$) [32]. As such we use the following ansatz with only one variation parameter, a:

$$\xi(\tau) = a^2\left\{1 - \exp\left[-\frac{\lambda^2\tau}{2a^2\beta\hbar}\left(1 - \frac{\tau}{\beta\hbar}\right)\right]\right\}. \tag{3.7}$$

This expression reduces to the free electron form at small τ and approaches a plateau value a at intermediate τ. We anticipate, and will show that, for large λ, a is much larger than all microscopic length scales and at the same time small compared to λ. In that case, $\xi(\tau) = \xi(\beta\hbar/2)$ for nearly all τ, and

$$\begin{aligned} R^2(\beta\hbar/2) &= 6\xi(\beta\hbar/2) \\ &= 6a^2. \end{aligned}$$

We also use Eq. (3.2) for $c(r)$, as is justified in Appendix B. As discussed in Appendix A, solving Eqs. (2.4)–(2.7) with the above approximations gives, to lowest orders of (l/a) and (σ/a),

$$\hat{c}(0) = -8\pi^{3/2}\hat{S}(0)^{-1}a^3\left[1 + 8\sqrt{\pi}Ka^3\Big/\hat{S}(0)\lambda^2 l\right]^{-1}. \tag{3.8}$$

In addition, it follows from Eqs. (A9) and (A10) that

$$\beta\Delta\mu_{\rm ref} + \langle S_{\rm ref}[\mathbf{r}(\tau)]\rangle_{\rm ref} = \frac{3\lambda^2}{8a^2}. \tag{3.9}$$

Substituting Eqs. (3.7), (3.8), and (3.9) into Eq. (2.9), (2.10), and (2.11) gives

$$\frac{\partial}{\partial a}\Delta\mu(a) = 0, \tag{3.10}$$

with

$$\begin{aligned} \Delta\mu(a) = {} & [4\pi^{3/2}\rho\hat{S}(0)^{-1}a^3][1 + 8\sqrt{\pi}Ka^3/\hat{S}(0)\lambda^2 l]^{-1} \\ & + \frac{3\lambda^2}{8a^2}. \end{aligned} \tag{3.11}$$

The result is a sixth-order polynomial equation in a:

$$16\pi^{3/2}\rho a^5/\hat{S}(0)\lambda^2 - [1 + 8\pi^{1/2}Ka^3/\hat{S}(0)\lambda^2 l]^2 = 0. \tag{3.12}$$

Real solutions exist when

$$\begin{aligned} &\hat{S}(0)^{-1/2}\rho^{-3/4}K^{5/4}l^{-5/4}\lambda^{-1} \\ &\qquad < 5^{5/4}\pi^{1/2}2^{-9/4}3^{-3/2}\ (= 0.536\ldots). \end{aligned} \tag{3.13}$$

For large λ, there is a unique asymptotic solution, given in Eq. (3.14) below. The smallest real root of Eq. (3.12) coincides with this solution. The smallest real root of this equation therefore gives the physical solution for a, and it is accurate away from the crossover region of the phase diagram, as is shown in Fig. 2.

By retaining only the lowest order terms in (a/λ), Eq. (3.12) gives a slightly generalized Lifshitz trap scaling behavior:

$$R = \sqrt{6}a \sim \frac{6^{1/2}\pi^{-3/10}}{2}\left[2\hat{S}(0)\lambda^2/\rho\right]^{1/5}, \tag{3.14}$$

and

$$\beta\Delta\mu \sim \frac{5}{4}(2\pi)^{3/5}\rho^{2/5}\hat{S}(0)^{-2/5}\lambda^{6/5}. \tag{3.15}$$

The generalization is the involvement of $\hat{S}(0)$. For uncorrelated disorder, $\hat{S}(0) = 1$. Notice that the distance

of closest approach l does not appear in the asymptotic expression, but only enters into higher order corrections. This universal behavior is a consequence of large cavities dominating the low energy states of the electron. For large cavities, the effect of the electron-solvent interaction is felt only at the surface of the cavities and becomes negligible compared to the bulk term. The temperature dependence of Eq. (3.15) is particularly noteworthy. Specifically, $\beta\Delta\mu$ is not a linear function of inverse temperature. Its fractional dependence, going as $\lambda^{6/5}$ in three dimensions, is a manifestation of the characteristic distribution of localized ground states for systems with disorder of finite correlation length and bounded lowest value of potential energy.

For a quantitative comparison, Luttinger *et al.* [29–31] calculated asymptotic results for an ideal gas which scatters the electron with a short-ranged, repulsive pseudopotential. (Specifically, in Ref. [31], they consider a repulsive power-law potential that decays faster than $1/r^5$.) Their excess chemical potential scales with ρ and λ in the same way as the one we have derived using an effective partition function, Eq. 2.8, but the numerical values differ by a factor of 2.5:

$$\beta\Delta\mu_{\mathrm{Lut}} \sim \frac{5}{6}(4\pi^4)\rho^{2/5}\lambda^{6/5} + O(\lambda^{4/5}),$$

$$\lambda \gg \rho^{-3/4}l^{-5/4}. \tag{3.16}$$

C. Crossover

The results of the previous two subsections demonstrate that the RISM-polaron theory is qualitatively correct in both limiting regimes. The strong-coupling regime prevails at a given temperature and solvent density if its excess chemical potential is lower than that of weak-coupling behavior. We compare these two excess chemical potentials given respectively by Eqs. (3.3) and (3.11) to obtain the crossover line, expressed as $\lambda_c(\rho_c)$. The result is

$$\rho_c l^2 \lambda_c \sim 3^{3/2}(2\pi)^{-1/2}\hat{S}(0)^{-1/2}\rho_c^{1/4}K^{5/4}l^{3/4}. \tag{3.17}$$

This expression is somewhat different from what is obtained by locating the crossover point from the temperature and density at which the ratio of λ to the mean free path, $\rho^{-1}\ell^{-2}$, reaches a threshold value. This "semiclassical" estimate yields $\rho_c\lambda_c \sim$ const. The correlation effects accounted for in arriving at Eq. (3.17) lead to a more complicated density dependence for the threshold to localization.

The competition between the factors of $\hat{S}(0)$ and K in Eq. (3.17) is significant. The factor K partially counteracts the effect of the bulk compressibility and can keep the strong-coupling regime favorable at high densities, even though $\hat{S}(0)$ is small in that regime. The crossover boundaries for several values of l obtained from Eq. (3.17) are shown in Fig. 4. In our model, for the range of parameters we have considered, increasing ρ always leads to stronger tendency of self-trapping [33]. The line predicted by Eq. (3.17) lies very close to the lower turning-points of the numerical curves exhibited for example in Fig. 2.

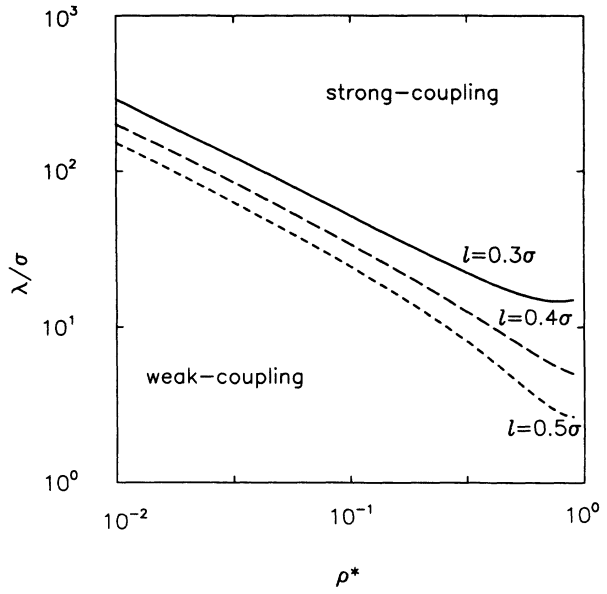

FIG. 4. Phase boundaries for pure excluded volume interaction: $l/\sigma = 0.3$ (solid line), 0.4 (long-dashed line) and 0.5 (dashed line). The lower left portion of the phase diagram is the weak-coupling regime and the upper right part corresponds to the strong-coupling regime.

IV. EFFECT OF ATTRACTIVE INTERACTION

A system with randomly placed sites that strongly attract (rather than repel) an electron forms Lifshitz traps of a different sort than those considered in Sec. III. These alternative traps are regions in which many strong attractors cluster. Points in space where they do not cluster will be locations of relatively high potential energy for the electron. Hence, the lowest energy electrons will be located in regions where the largest clusters of attractors reside. The phenomenological argument leading to Eq. (3.6) can be carried through for the case of strong attractors. The result is the same, except in this case in place of solvent concentration, ρ, one has a void concentration. The behavior of Lifshitz traps in the presence of strongly attracting particles therefore has roughly a mirror symmetry with that for Lifshitz traps in the presence of excluding particles.

With this symmetry in mind, consider systems where the randomly arranged particles possess both and expelling core as well as an attractive pseudopotential tail. If the expelling radius is small, and the attractive potential is deep, the system would create Lifshitz traps of the attracting type—we shall call them "cluster" states. On the other hand, if the attractions are weak, the exclusion will dominate, and the low energy electron will fill voids in the material—the Lifshitz trap "cavity" states analyzed in the previous section. The cluster state and the cavity state are different structures. One therefore ex-

pects that as the pseudopotential attraction is changed continuously from weak to strong, an intermediate regime will occur where the electron is neither associated with clusters nor voids. Such a situation would be a form of weak coupling. Indeed, we derive in this section a phase diagram with two distinct types of strong-coupling phases separated by a weak-coupling phase. The weak coupling arises from a cancellation between the attractive interactions and the exclusion forces. When this cancellation occurs, the electron mobility is very high.

To reach these results, we consider now the case where the attractive pseudopotential, $u(r)$, is no longer zero. We analyze first the weak-coupling regime, and then the strong-coupling regime. The crossover phase diagram we have just described is estimated as in Sec. III, by extrapolating the free energies of the two extremes to the points of intersection.

A. Weak-coupling regime

We again use Eq. (3.1) for $\xi(\tau)$ and solve for $c(r)$ as a functional of $u(r)$. The results (see Appendix A) are:

$$\beta\Delta\mu = \frac{\pi\rho\lambda^2 l}{2K}[1+B\mathcal{U}]^2 + \rho G\lambda^2 + \rho\beta\hat{u}(0). \tag{4.1}$$

where

$$\mathcal{U} = -\frac{\beta\hat{u}(0)}{\pi\lambda^2 l}, \tag{4.2}$$

$$B\mathcal{U} = -\frac{2\beta}{\pi^2\lambda^2}\int_0^\infty dk\,\hat{u}(k)\hat{S}(k)\frac{\sin kl}{kl}, \tag{4.3}$$

$$G = -\frac{\beta^2}{\pi^2\lambda^4}\int_0^\infty dk\,\hat{u}(k)^2\hat{S}(k), \tag{4.4}$$

and K is defined in Eq. (3.4). Since $\lambda^2 \propto \beta$, $\mathcal{U}$, B, G, and K are all independent of temperature. The chemical potential (4.1) differs from (3.3) in three ways. The last term in Eq. (4.1) is the mean field attractive energy between the electron and the unperturbed bulk fluid. The second term is a reaction-field correction that is usually small. These two contributions are present even for $l = 0$, i.e., when no excluded volume interaction is present.

The remaining difference involves the first term in Eq. (4.1). It is similar to but larger than the chemical potential of the pure excluded volume interaction case at weak coupling. The extra factor of $B\mathcal{U}$ can be interpreted as an additional restoring force that is renormalized into the short-ranged part of the effective coupling $c(r)$. This increased repulsive interaction comes about because the attractive forces draw the electron and solvent atoms closer together than when that force is absent. Equation (4.1) is different from the results of Springett-Jortner-Cohen theory. It results from a self-consistent treatment of the short-ranged excluded volume interaction and the longer-ranged attractive part of the pseudopotential in the presence of the liquid. The effective scattering length that results is density dependent.

B. Strong-coupling asymptotic results

For strong coupling to disorder, we again assume ground-state dominance at low temperatures [Eq. (3.7)] and carry through the calculations as before. In Appendix A we show that a is obtained by solving another polynomial equation, Eq. (A12), and that the chemical potential is given by Eq. (A11). To leading order in (a/λ), Eq. (A12) gives

$$a \sim \frac{\pi^{-3/10}}{2}\left(\frac{2\hat{S}(0)\lambda^2}{\rho}\right)^{1/5}\mathcal{V}[\rho;u(r)]^{-2/5}, \tag{4.5}$$

where

$$\mathcal{V}[\rho;u(r)] = 1 + (B-K)\mathcal{U} \tag{4.6}$$

is temperature independent. In other words, we predict that the electron size scales the same way with temperature as in the case for purely repulsive scatterers, but the coefficients, even to leading order in λ, are functionals of $u(r)$ and are not universal. This behavior follows from the fact that solvent atoms exist in the vicinity of the electron whenever $\mathcal{U} > 0$, in contrast to the case of pure excluded volume interaction where the electron resides in a cavity and the electron-atom pseudopotential contributes only to surface terms. These structural distinctions are quantified in the next subsection.

At large λ, the chemical potential, Eq. (A11), has the asymptotic form

$$\begin{aligned}\beta\Delta\mu &\sim 4\pi^{3/2}\rho\hat{S}(0)^{-1}\mathcal{V}[\rho;u(r)]^2a^3 + \frac{3\lambda^2}{8a^2} + \pi\rho\lambda^2 l(1+B\mathcal{U})\mathcal{U} - \frac{\pi\rho\lambda^2 l}{2}K\mathcal{U}^2 + \rho G\lambda^2 + \rho\beta\hat{u}(0)\\ &= \frac{5(2\pi)^{3/5}}{4}\rho^{2/5}\hat{S}(0)^{-2/5}|\mathcal{V}[\rho;u(r)]|^{4/5}\lambda^{6/5} - \frac{\pi\rho\lambda^2 l}{2K}\mathcal{V}[\rho;u(r)]^2 + \frac{\pi\rho\lambda^2 l}{2K}(1+B\mathcal{U})^2 + \rho G\lambda^2 + \rho\beta\hat{u}(0).\end{aligned} \tag{4.7}$$

It reduces to Eq. (3.15) when $\mathcal{U} = 0$. On comparing Eq. (4.7) with Eq. (3.15), one sees that the first term, of $O(\lambda^{6/5})$, is responsible for the Lifshitz-like scaling of the electron size. The terms proportional to the inverse temperature, $\beta \sim \lambda^2$, can be viewed as simply shifting the "zero" of energy with respect to the pure excluded volume case.

C. Phase diagram and distinct strong-coupling phases

The condition for strong coupling follows from comparing Eq. (4.1) and Eq. (A11) in Appendix A. It is given by

$$\rho_c l^2 \lambda_c > 3^{3/2}(2\pi)^{-1/2}\hat{S}(0)^{-1/2}\rho_c^{1/4} \times |\mathcal{V}[\rho; u(r)]|^{-3/2} K^{5/4} l^{3/4}. \quad (4.8)$$

This condition reduces to Eq. (3.17) in the case of purely excluded volume interaction.

Since $u(r)$ is finite, though discontinuous at $r = l$, $\hat{u}(k) \sim 1/k^2$. This decay is much faster than that of the Fourier transform of the $c(r)$ δ function. As a result, for reasonable $u(r)$'s and $\hat{S}(k)$'s,

$$B\mathcal{U} = \frac{2\mathcal{U}}{\pi}\int_0^\infty dk \frac{\hat{u}(k)}{\hat{u}(0)}\frac{\sin kl}{k}\hat{S}(k) \le \frac{2\mathcal{U}}{\pi l}\int_0^\infty dk \left(\frac{\sin kl}{k}\right)^2 \hat{S}(k) = K\mathcal{U}.$$

Hence, $\mathcal{V}[\rho; u(r)]$ decreases smoothly with increasing strength of the attractive potential $\mathcal{U}$, passes through zero and eventually changes sign, and its absolute value first increases and then decreases with increasing $\mathcal{U}$.

On the other hand, Eq. (4.8) states that small $|\mathcal{V}[\rho; u(r)]|$ favors the weak-coupling regime, whereas large values favor strong-coupling behavior. As a result, at large λ, ρ, and/or l, the system crosses over from the strong-coupling phase we studied in Sec. III to the weak-coupling regime. This crossover occurs in the neighborhood of densities where $\mathcal{V}[\rho; u(r)] \approx 0$. Therefore, the system exhibits a re-entrance into the strong-coupling regime as $\mathcal{U}$ increases from zero. Such crossover boundaries, obtained from Eq. (4.8), are illustrated in Fig. 5. In accordance with the physical argument given at the beginning of Sec. IV, we expect the strong-coupling phase with small $\mathcal{U}$ to be dominated by cavity states; and we expect the strong-coupling phase with large $\mathcal{U}$ to be dominated by cluster states.

The distinction between the two strong-coupling regimes is illustrated by the electron-solvent pair correlation function

$$h_{es}(r) = g(r) - 1. \quad (4.9)$$

In Fig. 6 we take $u(r)$ to be a simple, truncated charge-induced dipole interaction

$$u(r) = -\alpha e^2/2r^4, \; r > l,$$

where α is the renormalized polarizability of the solvent atoms and e is the electronic charge [34]. With this

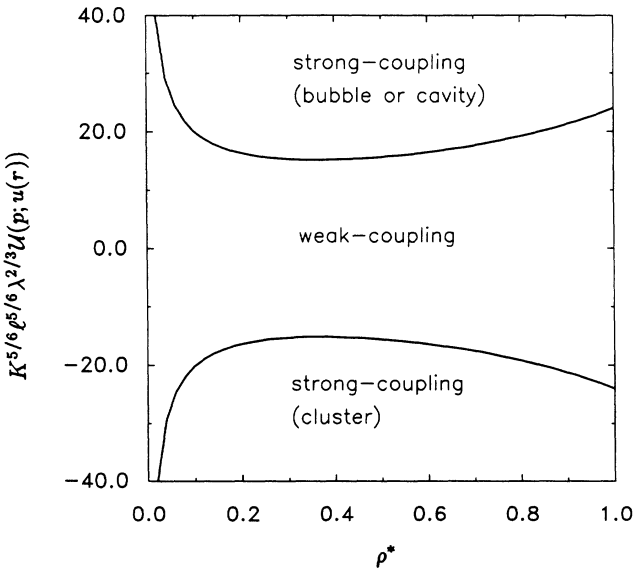

FIG. 5. Phase boundaries with both excluding and attracting interactions, expressed in terms of $K^{5/6}l^{5/6}\lambda^{2/3}\mathcal{V}[\rho; u(r)]$ as a function of $\rho\sigma^3$. The upper and lower branches correspond to the boundaries separating the weak-coupling from the bubble and cluster state.

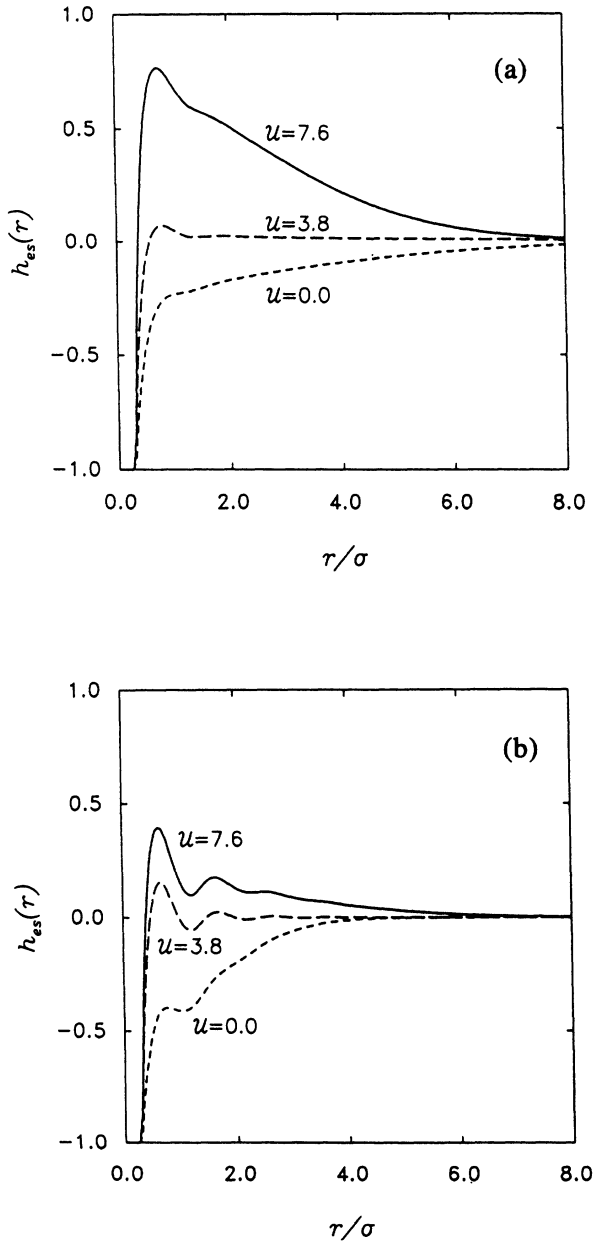

FIG. 6. $h_{es}(r)$ vs r for cases where $l = 0.29\sigma$: $\mathcal{U} = 7.6$ (solid line), 3.8 (long-dashed line), and 0 (dashed line). Panels (a) and (b) are for $\rho\sigma^3 = 0.3$ and 0.7, respectively.

potential, we plot numerically computed $h_{es}(r)$ at various values of $\mathcal{U}$. The distance of closest approach l is 0.29σ and $\lambda = 20\sigma$. At small $\mathcal{U}$, the excluded volume interaction dominates and we observe depletion of solvent density around the excess electron. As $\mathcal{U}$ increases, the "correlation-hole" disappears and the solvent effectively decouples from the electron, becoming transparent to it. At large $\mathcal{U}$, the local solvent density around the electron is much higher than the bulk value. The prediction of such clustering is not without precedence. Anionic clusters of xenon atoms are known to form experimentally [35]. Enhanced electron-solvent correlation are also observed in simulation of excess electrons in xenon [14(c)]. We further note that more pronounced local solvent structures exist near the electron at high solvent densities.

Another quantity of interest is the average number of solvent atoms correlated with the excess electron,

$$N_{corr} = -4\pi \int_0^\infty dr\, r^2 h_{es}(r) = -\hat{\omega}(0)\hat{c}(0)\hat{\chi}(0). \tag{4.10}$$

Equations (4.10), (A8), and (A14) imply that asymptotically the sign of N_{corr} is entirely determined by the function $\mathcal{V}[\rho; u(r)]$ in both the strong-coupling and the weak-coupling regime. A negative value for N_{corr} (e.g., near the pure excluded volume limit, where $\mathcal{V}[\rho; u(r)] = 1$) indicates the interaction is mainly of the excluded volume type. Conversely, if $\mathcal{U}$ is sufficiently large, $\mathcal{V}[\rho; u(r)]$ becomes negative in sign, which is the signature of systems where attractive forces dominate.

Keep in mind that one cannot distinguish between strong-coupling and weak-coupling behavior by looking at $h_{es}(r)$ alone. The correlation holes and enhanced electron-solvent correlations persist even in the weak-coupling regime. $h_{es}(r)$ indicates only whether attractive or repulsive interaction dominates. The same is true for N_{corr}. At sufficiently low temperature, however, sharp changes in $h_{es}(r)$'s accompany the sharp crossover between the different regimes. This will be clearly discernible if $h_{es}(r)$ is plot over a range of densities or temperatures.

For physical systems, $\mathcal{U}$ is a function of the electron-solvent pseudopotential and does not change drastically with thermodynamic conditions. To study the effect of solvent density on excess electrons for a particular solvent we assume $\mathcal{U}$ to be constant [36]. Suppose for a given $\mathcal{U}$ there exists a density ρ^* at which $|\mathcal{V}[\rho; u(r)]|$ has a minimum small enough to place the system in the weak-coupling regime. As ρ is tuned away from ρ^*, the tendency for strong-coupling behavior increases. In other words, the function $\mathcal{V}[\rho; u(r)]$ determines the feasibility of nonmonotonic equilibrium behavior of the electron-solvent system as a function of solvent density ρ. This is the concrete statement regarding the "cancellation" between attractive and repulsive interactions in our theory.

The quantitative predictions of this theory will not hold at arbitrarily strong attractive interactions for real physical fluids, as the fluid must cease to respond harmonically to sufficiently strong perturbations. The peak height near $r = l$ in $h_{es}(r)$ can be taken as a measure of the departure of the local solvent density from its bulk value. An unphysically large peak may be a signature of artifacts due to the approximate nature of the theory. This theory certainly fails for charge-dipole or unscreened Coulombic interaction between electron and solvent (see Appendix B). It is most accurate for long-ranged attractive potential, and also at high solvent densities at which the small compressibility limits density fluctuations and makes the Gaussian bath assumption valid.

D. Mobility in weak-coupling regimes

The analytic tools developed previously also give a simple expression for the position of the mobility peak. Following Ref. [10], at high mobility we make the free electron approximation in Eq. (2.20),

$$\xi_>^{free}(t - i\beta\hbar/2) = (\lambda^2/2)[1/4 + (t/\beta\hbar)^2]. \tag{4.11}$$

With this functional form, the t integral in Eq. (2.22) can be performed explicitly, and we obtain, via Eqs. (2.21) and

$$\frac{1}{D} = -\frac{\beta\hbar}{6\pi\sqrt{2\pi}\lambda} \int_0^\infty dk\, k^3 \hat{v}(k) e^{-k^2\lambda^2/8}. \tag{4.12}$$

At large λ we obtain

$$\frac{1}{D} = -(8\sqrt{2}/3\pi^{3/2})(\beta\hbar/\lambda^5)\hat{v}(k_0) + O(\lambda^{-3}), \tag{4.13}$$

where $k_0 = 2\sqrt{3}/\lambda$.

Our weak-coupling mobility result is analogous to the Cohen-Lekner result [37] for drift velocity of excess electrons, but with a "scattering length" generalized; our expression is reminiscent of the Basak and Cohen theory [38] in its dependence upon the structure of the fluid. Experimental data exhibiting this mobility maximum has been successfully fit by Simon *et al.* [39] employing a theory perhaps not inconsistent with this consensus. The maximum mobility as a function of $\mathcal{V}[\rho; u(r)]$ occurs approximately at the density where

$$\hat{v}(k_0) \approx \hat{v}(0) \propto \mathcal{V}[\rho; u(r)] = 0. \tag{4.14}$$

Further, the discussion at the end of the last subsection implies that if for a given $\mathcal{U}$, a sharp minimum exists in $\mathcal{V}[\rho; u(r)]$ as a function of ρ then electron mobility will exhibit a peak as a function of ρ. Since $\mathcal{V}[\rho; u(r)]$ is independent of λ, we predict no temperature dependence on the position of the peak at sufficiently low temperatures. The peak position as a function of temperature has not been systematically studied by experiment. Limited examination indicates only a slight temperature dependence for excess electrons in neopentane (Fig. 2.14b in Ref. [1(c)]).

Figure 7 displays a few slices of the $\mathcal{U}$-ρ-λ phase diagram as well as the lines of maximum mobility as predicted by Eq. (4.14). The boundaries are computed from

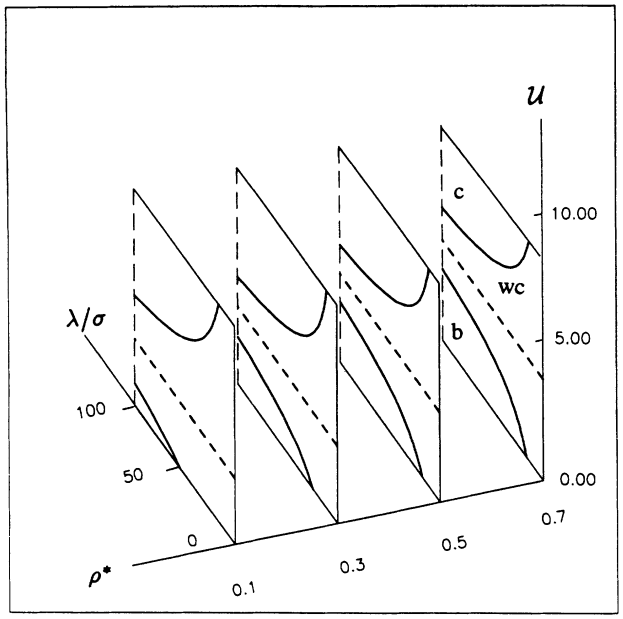

FIG. 7. Slices of the three-dimensional phase diagram calculated with a truncated $u(r) = -\alpha/2r^4$ attractive potential (see text). The solid curves are the phase boundaries separating the weak-coupling (wc) regimes and the cluster (c) and bubble (b) states. The dashed line is the line of maximum mobility [Eq.(4.14) in text].

Eq. (4.8). Here "b" refers to the cavity or "bubble" phase, "c" is the cluster phase, and "wc" denotes the weak-coupling regime. Higher solvent density not only narrows the weak-coupling region but also shifts it (as well as the location of the line of maximum mobility) to higher values of U [36].

From both Figs. 5 and 7, we see re-entrant behavior as a function of ρ with λ and U fixed. For example, the system goes from the "cluster" state to the weak-coupling regime and back again as ρ increases. This implies that the equilibrium size of the electron is a nonmonotonic function of density along certain isotherms in phase space, which is again indicative of the nontrivial competition between attractive and repulsive parts of the electron-solvent interaction.

V. CONCLUSION

In this paper we have arrived at approximate analytical expressions that describe the phase diagram and predict the location of maximum mobility. We have demonstrated that the RISM-polaron theory reproduces the correct Lifshitz trap scalings in the case of excluded volume interactions. For interactions dominated by effective attractive forces we predict a new type of Lifshitz trap behavior whereby the electron is localized in clusters of high solvent density. We believe that such cluster states should play a role in the correct interpretation of mobility experiments for highly polarizable fluids such as krypton, xenon, and certain organic fluids.

The RISM-polaron theory assumes a Gaussian bath. Such a model for the solvent in principle allows arbitrarily large density fluctuations, and, even when solvent-solvent correlation is taken into account through the static structure factor, this model is incapable of rigorously enforcing the solvent-solvent exclusion. For such a model bath, and for purely attractive interactions between electron and solvent [i.e., no excluded volume interaction, $l = 0$, with $u(r)$ integrable], the electron size would be small at sufficiently low temperatures for a given $u(r)$. The situation is similar to the problem of a quantum particle in a system of random uncorrelated attractors studied by Luttinger and Waxler [31]—the lowest lying states would be centered around small, dense clusters of attractors. As a result, our asymptotic arguments based on separation of length scales no longer apply, and there would be no Lifshitz-like scaling. This can be directly deduced from Eq. (4.8), which cannot be satisfied for $l = 0$.

Our theory predicts that, in a statistical sense, the presence of excluded volume interaction between electron and solvent prevents the formation of small, energetically-favorable cluster states and prevents the collapse of the excess electron. The repulsive part of the potential provides the "restoring force" that gives rise to an excess pressure, just as in the case with pure excluded volume interaction, resulting in a Lifshitz-like scaling. This prediction is irrespective of the structure of the solvent and also applies to an ideal gas solvent, in so far as the density fluctuations in an ideal gas can be adequately described as Gaussian. The crucial assumption seems to lie in approximating the solvent density fluctuation as Gaussian. It is expected that this assumption holds for incompressible systems in general, and also (for cluster states) in cases where the attractive part of the electron-solvent interaction is small enough that its effect on the solvent can be treated perturbatively, but is sufficiently large to cause formation of cluster states with Lifshitz-like scaling.

ACKNOWLEDGMENTS

This research has been supported in part by the National Science Foundation. We are grateful to Ken Hui for many helpful discussions. One of us (K.L.) has received financial support from the Department of Education.

APPENDIX A: ANALYTIC SOLUTION IN ASYMPTOTIC LIMIT

In this Appendix, we discuss the mathematical analysis used to derive the analytical solutions to Eqs. (2.4)–(2.6) and (2.14)–(2.18).

We consider the most general case, in which $c(r)$ contains an attractive tail contribution, $-\beta u(r)$. We recover the pure excluded volume result in the end by setting $u(r)$ to zero. Consider the strong-coupling ansatz in Eq. (3.7). For $\tau_1 = 2\beta\hbar a^2/\lambda^2$,

$$\xi(\tau) \approx \lambda^2\tau/2, \text{ for } 0 < \tau \leq \tau_1 \text{ or } (\beta\hbar - \tau_1) \leq \tau < \beta\hbar;$$

$$\xi(\tau) \approx a^2, \text{ for } \tau_1 \leq \tau \leq (\beta\hbar - \tau_1). \quad \text{(A1)}$$

We anticipate that $a \ll \lambda$ in the strong-coupling limit (see Fig. 2), and we will demonstrate that this is indeed a self-consistent assumption. Given this inequality, $\tau_1/\beta\hbar \ll 1$, and the crossover described by Eq. (A1) is sharp. We can in effect write

$$\exp[-k^2\xi(\tau)] = \exp(-k^2a^2) + \exp\left[-\frac{k^2\lambda^2\tau}{2\beta\hbar}\left(1 - \frac{\tau}{\beta\hbar}\right)\right] \quad \text{(A2)}$$

when performing k and τ integrations. At low temperatures we use

$$\hat{c}(k) = c_\delta \frac{\sin kl}{kl} - \beta\hat{u}(k). \quad \text{(A3)}$$

(See Appendix B.) c_δ is then determined by extremizing the following RISM functional [4]:

$$\frac{\partial}{\partial c_\delta} I_{\text{RISM}} = 0, \quad \text{(A4)}$$

where

$$I_{\text{RISM}} = \rho\hat{c}(0) + (\rho/4\pi^2\beta\hbar) \times \int_0^\infty dk\, k^2 \int_0^{\beta\hbar} d\tau\, \hat{c}^2(k)\hat{S}(k)e^{-k^2\xi(\tau)}. \quad \text{(A5)}$$

Applying Eq. (A2) to the τ integral above gives

$$\frac{1}{\beta\hbar}\int_0^{\beta\hbar} d\tau\, e^{-k^2\xi(\tau)} = e^{-k^2a^2} + \frac{4}{k^2\lambda^2}, \quad \text{(A6)}$$

plus terms of higher order in $1/\lambda$. Eq. (A6) is substituted into Eq. (A5). We note that $\hat{c}(k)$ and $\hat{S}(k)$ varies slowly compared with the first term of Eq. (A6) and can be approximated by their zero wavevector values. The corrections are of order (l/a) and (σ/a) and are neglected. The second term of Eq. (A6) is evaluated explicitly. Solving Eq. (A5) with these approximations gives

$$c_\delta = -8\pi^{3/2}\hat{S}(0)^{-1}[(1 + B\mathcal{U})a^3 + \hat{S}(0)\lambda^2 l\,\mathcal{U}/8\sqrt{\pi}] \times [1 + 8\sqrt{\pi}Ka^3/\hat{S}(0)\lambda^2 l]^{-1}, \quad \text{(A7)}$$

where K, $\mathcal{U}$, and B are defined in Eqs. (3.4), (4.2), and (4.3), respectively. From the definition of $\hat{c}(k)$, it follows that

$$\hat{c}(0) = -8\pi^{3/2}\hat{S}(0)^{-1}a^3\mathcal{V}[\rho; u(r)] \times [1 + 8\sqrt{\pi}Ka^3/\hat{S}(0)\lambda^2 l]^{-1}, \quad \text{(A8)}$$

where $\mathcal{V}[\rho; u(r)]$ is defined by Eq. (4.6). Equation (3.8) is obtained by setting $\mathcal{U} = 0$.

Next, we compute $\beta\Delta\mu_{\text{ref}} + \langle S_{\text{ref}}[\mathbf{r}(\tau)]\rangle_{\text{ref}}$. Performing the Gaussian functional integral over $S_{\text{ref}}[\mathbf{r}(\tau)]$ yields

$$\beta\Delta\mu_{\text{ref}} + \langle S_{\text{ref}}[\mathbf{r}(\tau)]\rangle_{\text{ref}} = 3\sum_{n=0}^{\infty}[\gamma_n/(\beta m_e\Omega_n^2 + \gamma_n) - \ln(\beta m_e\Omega_n^2 + \gamma_n)]. \quad \text{(A9)}$$

Equation (3.7) allows us to invert Eq. (2.14) explicitly, giving

$$\gamma_n = \lambda^2/4a^4 \quad \text{(A10)}$$

plus negligible corrections. With this expression for γ_n, Eq. (A9) reduces to Eq. (3.9). Finally,

$$\langle S_I\rangle_{\text{ref}} = I_{\text{RISM}}$$

is computed by performing τ and k integrations as before, and by applying Eq. (A8).

Putting all the terms together, the chemical potential becomes

$$\beta\Delta\mu(a) = [4\pi^{3/2}\rho\hat{S}(0)^{-1}(1 + B\mathcal{U})^2a^3 + \pi\rho\lambda^2 l(1 + B\mathcal{U})\mathcal{U} - \frac{\pi}{2}\rho K\lambda^2 l\mathcal{U}^2](1 + 8\sqrt{\pi}Ka^3/\hat{S}(0)\lambda^2 l)^{-1} + \rho G\lambda^2 + \rho\beta\hat{u}(0) + \frac{3\lambda^2}{8a^2}, \quad \text{(A11)}$$

where G is defined in Eq. (4.4). When $\mathcal{U}$ vanishes, Eq. (A11) becomes identical to Eq. (3.11). Minimizing the above expression for the chemical potential with respect to the parameter a gives a sixth-order polynomial equation in a:

$$16\pi^{3/2}\rho\mathcal{V}[\rho; u(r)]^2a^5/\hat{S}(0)\lambda^2 - [1 + 8\pi^{1/2}Ka^3/\hat{S}(0)\lambda^2 l]^2 = 0. \quad \text{(A12)}$$

In the asymptotic region, $a \sim \lambda^{2/5}$. Our assumption about the relative magnitudes of a and λ is therefore self-consistent. By keeping only lowest order terms in (a/λ) we recover the Lifshitz-type scaling in Eq. (4.5), which reduces to Eq. (3.14) when $\mathcal{U} = 0$.

Identical results can also be obtained in the strong-coupling regime by using a single harmonic oscillator reference action with frequency $\omega_o = \lambda^2/2a^2$. The specific form of the ansatz is unimportant as long as it has the correct long time and short time behavior.

A brief note on the approximations used in this Appendix suffices. All these equations are correct to the lowest order of (l/a), (σ/a), (L_u/a), (l/λ), (σ/λ), and (L_u/λ), where L_u is the length scale of $u(r)$. In addition, they are correct to all orders of (a/λ) *in so far* as Eq. (A2) holds. We do not truncate our expressions to a finite order in (a/λ) because it is nontrivial to estimate the corrections that go into Eq. (A2), and also because our expression for a interpolates successfully into the crossover region (again, see Fig. 2).

The preceding discussions apply only for the strong-coupling regimes. In the weak-coupling regime, there is no ground state dominance, and $\xi(\tau)$ is well approximated by Eq. (3.1) at short times. Substituting Eq. (3.1) into Eq. (A5) and using Eq. (A3) for $c(r)$ we obtain

$$c_\delta = -\pi\lambda^2 l[1 + B\mathcal{U}]/K, \quad \text{(A13)}$$

and

$$\hat{c}(0) = -\pi\lambda^2 l\mathcal{V}[\rho; u(r)]/K, \tag{A14}$$

as well as Eq. (4.1). For the pure excluded volume interaction problem, $\mathcal{U}$ and G vanish, and we recover Eq. (3.3).

APPENDIX B: FUNCTIONAL FORM OF $c(r)$

We show that either in the weak coupling regime or as λ becomes much larger than all other length scales, a δ function form for $c(r)$ is the correct solution that satisfies the core condition for the electron-solvent pair correlation function [Eq. (2.4)]. A direct corollary of this argument is that $c(r)$ is also adequately represented by a δ-function term in the strong-coupling regime. This is because, from Eq. (A2), $\omega(r)$ can be written as

$$\omega(r) \approx (\pi\lambda^2 r)^{-1}\exp(-2r^2/\lambda^2) + (8\pi^{3/2}a^3)^{-1}\exp(-r^2/4a^2)$$

in the latter regime. It can easily be shown that the second term smears out all functions of length scales l, and to leading order is independent of the form of $c(r)$. Consequently, it is again the free electron form for $\omega(r)$ that determines the form of $c(r)$ at short range in the strong-coupling regime.

We assume that $c(r)$ consists of a δ function and an analytic part for $r < l$:

$$c(r) = c_l(r),\ r < l,$$
$$= c_\delta \frac{1}{4\pi r^2}\delta(r-l) + \sum_{j=0}^{n} c_j (r/l)^j,\ r < l.$$

This assumption is self-consistent under conditions described below. We start from Eq. (2.4) with

$$c(r) = c_l(r),\ r < l,$$
$$c(r) = -\beta u(r),\ r > l,$$
$$\omega(r) = (\pi\lambda^2 r)^{-1}\exp(-2r^2/\lambda^2),$$
$$\chi(r)/\rho = \frac{1}{4\pi r^2}\delta(r) + \rho h_{ss}(r),$$

with $h_{ss}(r)$ being the bulk solvent-solvent pair correlation function, and derive conditions for $c_l(r)$ that satisfy Eqs. (2.4) and (2.5). We rewrite Eq. (2.4) as

$$\begin{aligned} h_{es}(r) = {} & \frac{2\pi}{r}\int_0^l dr'\, r' c_l(r') \int_{|r-r'|}^{r+r'} dr''\, r''\omega(r'') + \frac{2\pi}{r}\int_l^\infty dr'\, r'[-\beta u(r')]\int_{|r-r'|}^{r+r'} dr''\, r''\omega(r'') \\ & + \frac{2\pi}{r}\int_0^l dr'\, r' c_l(r')\int_{|r-r'|}^{r+r'} dr''\, r''\frac{2\pi}{r''}\int_0^\infty dr'''\, r'''\rho h_{ss}(r''')\int_{|r''-r'''|}^{r''+r'''} dr''''\, r''''\omega(r'''') \\ & + \frac{2\pi}{r}\int_l^\infty dr'\, r'[-\beta u(r')]\int_{|r-r'|}^{r+r'} dr''\, r''\frac{2\pi}{r''}\int_0^\infty dr'''\, r'''\rho h_{ss}(r''')\int_{|r''-r'''|}^{r''+r'''} dr''''\, r''''\omega(r'''') \\ \equiv {} & h_1(r) + h_2(r) + h_3(r) + h_4(r). \end{aligned} \tag{B1}$$

Expanding $\omega(r)$ to $O(\lambda^{-2})$, we obtain

$$\int_{|r-r'|}^{r+r'} dr''\, r''\omega(r'') = \frac{1}{\pi\lambda^2}\int_{|r-r'|}^{r+r'} dr''\, e^{-2r^2/\lambda^2} \approx 2\min(r,r')/\pi\lambda^2. \tag{B2}$$

Using this approximation, corrections to Eq. (B1) are of order $1/\lambda$ or smaller for $u(r)$ decaying as r^{-4} or faster. We find, for $r < l$,

$$h_1(r) = \frac{c_\delta}{\pi\lambda^2 l} + \frac{4}{\lambda^2}\sum_{j=0}^{n}\frac{c_j}{j+2}\left[l^2 - \frac{l^{-j}r^{j+2}}{j+3}\right],$$

$$h_2(r) = \frac{4}{\lambda^2}\int_l^\infty dr'\, r'[-\beta u(r')] \equiv \eta,$$

$$h_3(r) = \frac{2\rho c_\delta}{3\lambda^2}(6\kappa + l^2 + r^2) + \frac{8\pi\rho}{3\lambda^2}\sum_{j=0}^{n} c_j\left[\frac{6\kappa l^3}{j+3} + \frac{l^5}{j+5} + \frac{l^3 r^2}{j+3}\right],$$

and

$$h_4(r) = -\frac{8\pi}{\lambda^2 r}\int_l^\infty dr'\, W(r')\int_{r'-r}^{r'+r} dr''\, r''\rho h_{ss}(r''), \tag{B3}$$

where

$$\kappa = \int_0^\infty dr'\, r' h_{ss}(r'), \tag{B4}$$

and

$$W(r) = \int_r^\infty dr' \int_{r'}^\infty dr''\,[-\beta u(r'')]r''. \tag{B5}$$

From Eq. (B3), it is seen that $u(r)$ must decay faster than r^{-2}. Slower decay causes η to diverge.

To satisfy the core condition, Eq. (2.5), the coeffients for terms of $O(r^n)$ for positive integers n must vanish. Provided that $u(r) = 0$ (pure excluded volume interaction) or $h_{ss} = 0$ (ideal gas limit), we deduce that, to zeroth order in λ^{-1},

$$c(r) = (c_\delta/4\pi r^2)\delta(r-l) + c_0,\ r < l,$$

and

$$c_0 = \rho c_\delta/(1 - 4\pi\rho l^3/3).$$

Furthermore, notice that $c(r)$ enters into the calculation of the partition function via Eq. (2.10). Since the Fourier transform of the δ function is much longer ranged than that of the step function, at all reasonable densities the contribution of the c_0 term is no more than a few percent. This has been verified numerically for all cases of $\lambda \geq 10\sigma$ that we studied. Hence, we ignore the step-function term.

The last piece of Eq. (B3) cannot be expressed in closed form and is a nontrivial functional of $u(r)$. Indeed, in general this term is not an analytic function of r for $r < l$, and our assumption for $c_l(r)$ no longer holds. However, at low densities, and also for $u(r)$ that are of length scales much larger than σ, the contribution of $h_2(r)$ should be much greater than that from $h_4(r)$. This is evident if we rewrite $h_4(r)$ as follows:

$$h_4(r) = -\frac{2}{\pi^2\lambda^2 r}\int_0^\infty dk k \sin(kr)\hat{X}(k)\hat{h}_{ss}(k),$$

where $X(r) = W(r)/r$. This expression gives a constant with corrections in terms of (r/σ) and (r/L_u), with L_u being the length scale of the attractive potential. Analytically we cannot prove that these corrections are negligible for a general function $u(r)$, but empirically we find that the δ-function ansatz is justified for all cases of $\lambda \geq 10\sigma$ that we studied.

[1] See, for example, (a) R. A. Holroyd and W. F. Schmidt, Annu. Rev. Phys. Chem. **40**, 439 (1989); (b) W. F. Schmidt, IEEE Trans. Electr. Insul. **19**, 389 (1984); (c) G. R. Freeman, in *Kinetics of Nonhomogeneous Processes*, edited by G. R. Freeman (Wiley, New York, 1987), pp. 19–87.

[2] Many of the seminal ideas and early experimental results are described in the articles found in Can. J. Chem. **55**, 1795–2264 (1977).

[3] See, for example, (a) H. T. Davis and R. G. Brown, Adv. Chem. Phys. **31**, 329 (1975); (b) D. F. Coker and B. J. Berne, in *Excess Electrons in Dielectric Media*, edited by C. Ferradini and J.-P. Jay-Gerin (CRC, Boca Raton, 1991), pp. 211–257; (c) J. P. Hernandez, Rev. Mod. Phys. **63**, 675 (1991).

[4] D. Chandler, Y. Singh, and D. M. Richardson, J. Chem. Phys. **81**, 1975 (1984).

[5] A. L. Nichols, D. Chandler, Y. Singh, and D. M. Richardson, J. Chem. Phys. **81**, 5109 (1984).

[6] A. L. Nichols III and D. Chandler, J. Chem. Phys. **84**, 398 (1985).

[7] D. Laria and D. Chandler, J. Chem. Phys. **87**, 4088 (1987).

[8] A. L. Nichols III and D. Chandler, J. Chem. Phys. **87**, 6671 (1987).

[9] Y. Fan and B. N. Miller, J. Chem. Phys. **93**, 4322 (1990).

[10] D. Hsu and D. Chandler, J. Chem. Phys. **93**, 5075 (1990).

[11] A. Sethia and Y. Singh, Phys. Rev. B **42**, 6090 (1990).

[12] D. Laria, D. Wu, and D. Chandler, J. Chem. Phys. **95**, 4444 (1991).

[13] A. Sethia and Y. Singh, Phys. Rev. B **46**, 9958 (1992).

[14] See, for example, (a) J. Lekner, Phys. Rev. Lett. **27A**, 341 (1968); (b) J. A. Jahnke, L. Meyer, and S. A. Rice, Phys. Rev. A **3**, 734 (1971); (c) D. F. Coker, B. J. Berne, and D. Thirumalai, J. Chem. Phys. **86**, 5689 (1987); (d) B. Space, D. F. Coker, Z. H. Liu, B. J. Berne, and G. Martyna, *ibid.* **97**, 2002 (1992); (e) J.-M. Lopez-Castillo, Y. Frongilla, B. Plenkiewicz, and J.-P. Jay-Gerin, *ibid.* **96**, 9092 (1992); (f) J. Meyer and R. Reininger, Phys. Rev. A **47**, R3491 (1993).

[15] C. Ramsauer, Ann. Phys. (Leipzig) **64**, 513 (1921); **66**, 545 (1921); **72**, 345 (1923); C. Ramsauer and R. Kollath, Ann. Phys. **3**, 536 (1929).

[16] D. H. Dunlap, H-L. Wu, and P. Phillips, Phys. Rev. Lett. **65**, 88 (1990); P. Phillips and H-L. Wu, Science **252**, 1805 (1991). P. K. Datta, D. Giri, and K. Kundu, Phys. Rev. B **47**, 10727 (1993).

[17] M. E. Cates and R. C. Ball, J. Phys. (Paris) **49**, 2009 (1988).

[18] B. Space and D. F. Coker, J. Chem. Phys. **94**, 1976 (1991); **96**, 652 (1992).

[19] H. Li and M. Kardar, Phys. Rev. A **46**, 6490 (1992); Phys. Rev. Lett. **67**, 3275 (1991).

[20] D. Chandler, Phys. Rev. E **48**, 2898 (1993).

[21] R. P. Feynman, Phys. Rev. **97**, 660 (1955).

[22] Numerically, Eqs. (2.4)–(2.6), (2.13)–(2.17) are solved iteratively according to the work of Nichols *et al.* [5]. In that work $c(r)$ is expanded in an appropriate basis set:

$$c(r) = c_\delta \frac{1}{4\pi r^2}\delta(r-l) + \sum_{j=0}^{n} c_j (r/l)^j, \; r < l.$$

The delta-function basis function gives rise to a long-ranged $1/k$ term in $\hat{c}(k)$, and whenever possible the contribution of this term is subtracted out and added back in analytically. This is facilitated by our knowledge that

$$e^{-k^2\xi(\tau)} \sim e^{-\lambda^2 k^2 \tau/(2\beta\hbar)}, \; \tau \to 0$$

irrespective of ρ.

[23] D. Chandler, in *The Liquid State of Matter: Fluids, Simple and Complex*, edited by E. W. Montroll and J. L. Lebowitz (North Holland, Amsterdam, 1982), pp. 275–340.

[24] M. S. Wertheim, Phys. Rev. Lett. **10**, 321 (1963); E. Thiele, J. Chem. Phys. **39**, 474 (1963).

[25] C. C. Grimes and G. Adams, Phys. Rev. B **41**, 6366 (1990).

[26] B. E. Springett, J. Jortner, and M. H. Cohen, J. Chem. Phys. **48**, 2720 (1968); see also the subsection titled "Conduction Band Energy" in Ref. [1(a)], and references cited therein.

[27] E. Wigner and F. Seitz, Phys. Rev. **43**, 804 (1933); **46**, 509 (1934).

[28] I. M. Lifshitz, Usp. Fiz. Nauk **83**, 617 (1964) [Sov. Phys. Usp. **7**, 549 (1965)].

[29] R. Friedberg and J. M. Luttinger, Phys. Rev. B. **12**, 4460 (1975).

[30] J. M. Luttinger and R. Tao, Ann. Phys. **145**, 185 (1982).

[31] J. M. Luttinger and R. Waxler, Ann. Phys. **175**, 319 (1987).

[32] D. Chandler, in *Les Houches, Part 1, Liquids, Freezing and the Glass Transition*, edited by D. Levesque, J. P. Hansen, and J. Zinn-Justin (Elsevier, Amsterdam, 1991), pp. 193–285.

[33] See C. L. Cleveland and G. A. Gersch, Phys. Rev. A **23**, 261 (1981), and Sethia and Singh, [13]. We note that increasing density of solvent always leads to stronger tendency of self-trapping within the region of phase space we studied. This is contrary to the predictions of Cleveland and Gersch who predict a re-entrance into weak-coupling regime from strong-coupling regime at high solvent densities along certain isotherms. In terms of our theory the occurance of this phenomenon should be sensitive to the ρ dependence of the liquid structure factor. Using the RISM-polaron theory reviewed in this paper, Sethia and Singh observe a sharp increase in $\xi(\beta\hbar/2)$ at $l = 0.29\sigma$ and $\lambda = 15\sigma$ as ρ increases to sufficiently large values, indicative of re-entrance into weak-coupling regime. Our own conclusion is that this weak-coupling branch of their solution is "meta-stable"; in other words there exists a strong-coupling solution at lower free energy than the one they observe. Our results suggest that the re-entrant phenomenon predicted by Cleveland and Gersch is possibly an artifact of the approximate treatment of their model.

[34] The asymptotic expressions arrived at in Appendix A and quoted in the previous subsection are very accurate when compared with the full numerical solution when a short-ranged attractive potential is present. However, the potential we use has a slowly-decaying algebraic tail. Consequently, $\hat{u}(k)$ decays rather quickly at small wavevectors (linearly in k), and as a result the full numerical results and the analytical ones agree to only about 10% even when λ is very large. Better agreement can be obtained if we explicitly use $\hat{u}(k) \sim \hat{u}(0) + \hat{u}'(0)k$ in Eq. (A5). This improvement would not change the qualitative result of our phase diagram, Fig. 7.

[35] H. Haberland, T. Kolar, and T. Reiners, Phys. Rev. Lett **63**, 1219 (1989).

[36] Note that, in reality, $\mathcal{U}$ should be a weak function of ρ. Because of the many-body screening effect, the effective polarizability of atoms in a real fluid decreases with density; see for example [14(d)].

[37] J. Lekner, Phys. Rev. **158**, 130 (1967); M. H. Cohen and J. Lekner, *ibid.* **158**, 305 (1967).

[38] S. Basak and M. H. Cohen, Phys. Rev. B **20**, 3404 (1979).

[39] S. H. Simon, V. Dobrosavljevil, and R. M. Stratt, J. Chem. Phys. **94**, 7360 (1991).